

Origin of Pyroelectricity in LiNbO₃

Qing Peng and R. E. Cohen

Geophysical Laboratory, Carnegie Institution of Washington, 5251 Broad Branch Road NW, Washington, D.C., 20015, U.S.A.

We use molecular dynamics with a first-principles based shell model potential to study pyroelectricity in lithium niobate. We find that the primary pyroelectric effect is dominant, and pyroelectricity can be understood simply from the anharmonic change in crystal structure with temperature and the Born effective charges on the ions. This opens a new experimental route to studying pyroelectricity, as candidate pyroelectric materials can be studied with X-ray diffraction as a function of temperature in conjunction with theoretical effective charges. We also predict an appreciable pressure effect on pyroelectricity, which could be used to optimize materials pyroelectricity, and the converse electrocaloric effect, peak as T_c is approached.

PACS numbers: 77.70.+a, 77.84.Ek, 31.15.xv, 71.15.Pd

The theory of ferroelectricity had a classical period that culminated in the 1970s [1–3], followed by a quiescent period, and was rejuvenated in the 1990s with the introduction of modern electronic structure methods to these complex, interesting, and useful materials [4, 5]. The fundamental physics of pyroelectricity, the change in polarization with respect to temperature, has not been re-investigated until now, and there is no previous first principles computation of pyroelectricity. Pyroelectricity is of current great interest since the discovery of particle acceleration of ions from changes in temperature at pyroelectric surfaces sufficient to generate hard X-rays in a commercial product [6–8] as well as neutrons in heavy water via fusion [9]. LiNbO₃ is a uniaxial pyroelectric with space group R3c in the polar phase with ten atoms per primitive cell, and a T_c of 1480K [1, 10]. The structure, polarization and lattice dynamics of LiNbO₃ have been previously studied from first-principles using total energy, Berry's phase and linear response methods within Density Functional Theory (DFT) [10–12]. LiNbO₃ has been studied extensively experimentally [1, 13] due to its use in SAW filters and non-linear optics. There is also much interest now in the converse of the pyroelectric effect, the electrocaloric effect, for refrigeration or energy scavenging. [14–16]

Pyroelectricity is the change in spontaneous polarization P_s with temperature T . The total pyroelectric coefficient is

$$\Pi = \frac{dP_s}{dT} = \left(\frac{\partial P_s}{\partial T}\right)_\epsilon + \left(\frac{\partial P_s}{\partial \epsilon}\right)_T \left(\frac{\partial \epsilon}{\partial T}\right)_\sigma = \Pi_1 + \Pi_2. \quad (1)$$

The first term on the right side is the primary pyroelectric effect and the second the secondary effect. Experimentally the pyroelectric effect is measured under the constraint of constant stress. The experimentally accessible or proper pyroelectric coefficient is due to the adiabatic current flow J due to a slow change in temperature, $\Pi' = \frac{dJ}{dT}$, where T is the change in temperature T with time t . The Π' of an unclamped sample can be expressed

as

$$\Pi' = \Pi_1 + \Pi_2 + \Pi_3. \quad (2)$$

Π_1 measures the variation of spontaneous polarization with respect to temperature at constant strain (clamped), which arises from changes in phonon occupations and anharmonicity. Π_2 is the result of crystal deformation where the strain caused by thermal expansion alters the polarization via the piezoelectric effect as $\Pi_{2i} = \alpha_{jk} c_{jklm} d_{ilm}$, where the indices label coordinate directions [17], repeated indices imply summation, d_{ilm} are piezoelectric compliances, c_{jklm} are elastic moduli, and α_{ij} are the thermal expansion coefficients. $\Pi_3 = 2\alpha_1 P_s$ is the difference from the total and proper pyroelectric coefficients [1], where α_1 is the linear thermal expansion coefficient of the plane perpendicular to the polar axis. Π' can be measured with charge-integration or dynamic pyroelectric techniques [1], whereas Π_1, Π_2, Π_3 cannot be measured directly. Understanding the components of Π_1, Π_2, Π_3 is crucial in studying pyroelectricity and its origin.

We performed density functional theory (DFT) computations and fitted the results to a atomistic shell model. We used Density Functional Perturbation Theory (DFPT) [18] to compute phonons, effective charges, and dielectric constants. We performed first principles calculations with the *ABINIT* package [19] within the local density approximation (LDA) [20]. Lithium 1s and 2s electrons, niobium 4s, 4p, 4d, and 5s electrons, as well as oxygen 2s and 2p electrons were considered as valence states. We constructed pseudopotentials using the *OPIUM* package [21]. We used a kinetic energy cutoff of 45 Hartree and sampled the Brillouin zone using a $6 \times 6 \times 6$ Monkhorst-Pack mesh of special k points. The results were carefully checked against previous all-electron [10] and pseudopotential [11, 12] computations.

The structural parameters of LiNbO₃ in its polar ground state as functions of volume were obtained by relaxing the cell shape and atomic positions at seven volumes from 92.55 to 110.19 Å³ (5 to 20 GPa from the

TABLE I. First principles calculation of structure, spontaneous polarization P_s , constant volume specific heat capacity C_v , volumetric thermal expansivity α of LiNbO_3 using DFPT and the ABINIT code.

	a_H (Å)	c_H (Å)	P_s (C/m ²)	C_v (J/molK)	α (10 ⁻⁵ /K)
DFT(0K)	5.151	13.703	0.86		
QHLD(300K)	5.184	13.774		94.04	3.59
MD(300K)	5.145	13.488	0.63		2.63
Exp.(300K)	5.151 ^a	13.876 ^a	0.70-0.71 ^b	95.8 ^c	3.24-3.83 ^d

a [22]; b [2, 23]; c [24]; d [25–27]

TABLE II. First principles calculation of the elastic moduli c , piezoelectric strain constants d and piezoelectric stress constants e of LiNbO_3 using DFPT and the ABINIT code.

	Smith <i>et al.</i> [27]	Yamada [31] <i>et al.</i>	Present
c	($\times 10^{11}$ N/m ²)	($\times 10^{11}$ N/m ²)	($\times 10^{11}$ N/m ²)
c_{11}	2.030	2.03	2.18
c_{12}	0.573	0.53	0.68
c_{13}	0.752	0.75	0.78
c_{14}	0.085	0.09	0.15
c_{33}	2.424	2.45	2.40
c_{44}	0.595	0.60	0.55
c_{66}	0.728	0.75	0.75
d	($\times 10^{-11}$ C/N)	($\times 10^{-11}$ C/N)	($\times 10^{-11}$ C/N)
d_{15}	6.92	6.8	8.12
d_{22}	2.08	2.1	2.37
d_{31}	-0.09	-0.1	-0.15
d_{33}	0.60	0.6	0.81
e	(C/m ²)	(C/m ²)	(C/m ²)
e_{15}	3.76	3.7	3.722
e_{22}	2.43	2.5	2.317
e_{31}	0.23	0.2	0.219
e_{33}	1.33	1.3	1.718

fitted equation of state). We also optimized the atomic coordinates for the paraelectric symmetry $R\bar{3}c$ with the same sets of optimized lattices.

We computed the phonon frequencies using DFPT on a $4 \times 4 \times 4$ grid of q-points at each of the seven volumes. The frequencies were interpolated onto a finer grid using short-range force constants [28]. Quasi-harmonic Helmholtz free energies were obtained from these frequencies as functions of temperature and volume. Isotherms were fitted to the Vinet equation of state [29].

The polarization was computed for each of the seven volumes using the Berry's phase method with a $4 \times 4 \times 20$ mesh of k points. The results of the calculations were checked for convergence with respect to the number of k points and the plane wave cutoff energy. We obtained P_s as the differences of the polarization between the polar and centrosymmetric LiNbO_3 at each volume, making sure we are on the same polarization versus mode coordinate curve [30].

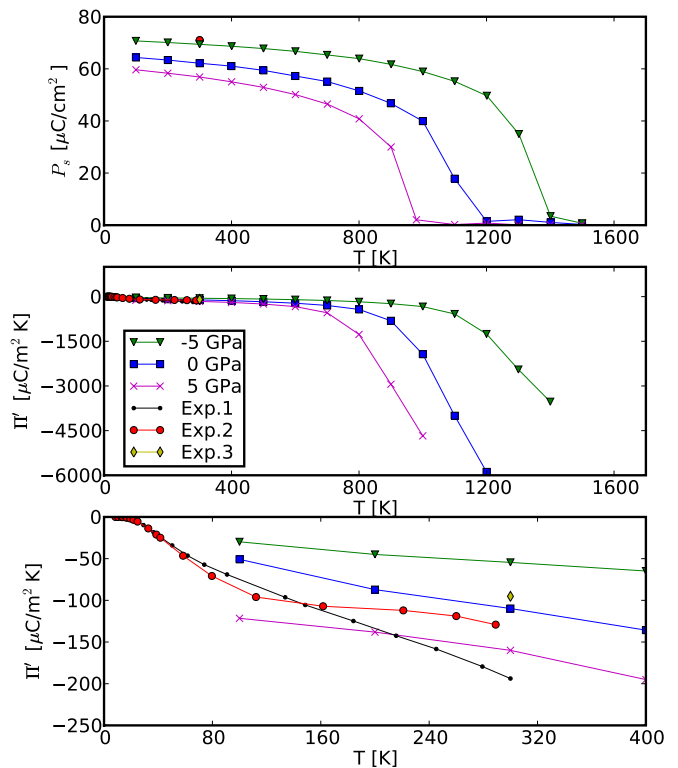


FIG. 1. Molecular dynamics simulation results for LiNbO_3 in the $N\sigma T$ ensemble. The results for $P = -5, 0, 5$ GPa are presented by triangle, square, and cross line respectively. Exp.1 is the experimental value of congruent sample in ref. [2]. Exp.2 is stoichiometric sample in ref. [2]; Exp.3 is experiment in ref. [32]. Note that our results from classical MD, so Π' does not go to zero at zero temperature as required by quantum mechanics.

The shell model approach has proven to be a computationally efficient and confident methodology for the simulation of ferroelectric perovskites, including bulk properties of pure crystals, solid solutions and super lattices, and also surfaces and thin films properties[33]. In this model, each atom is represented by a massive core coupled to a massless shell, and the relative core-shell displacement describes the atomic polarization. The model contains 4th order core-shell couplings, long-range Ewald interactions and short-range interactions described by the Rydberg potential $V(r) = (a + br) \exp(r/\rho)$. The parameters were fit from the DFT and DFPT results of total energies, forces, stresses, phonon frequencies and eigenvectors, Born effective charges, and dielectric constants for a number of distorted and strained structures. We then performed classical molecular dynamic simulations with *DL_POLY* package [34].

We computed the spontaneous polarizations P_s during the MD simulations. $N\sigma T$ ensembles in MD simulations capture the evolutions of the system volume and shape corresponding to applied pressure, temperature. As a result, MD simulations in $N\sigma T$ ensemble allow us to com-

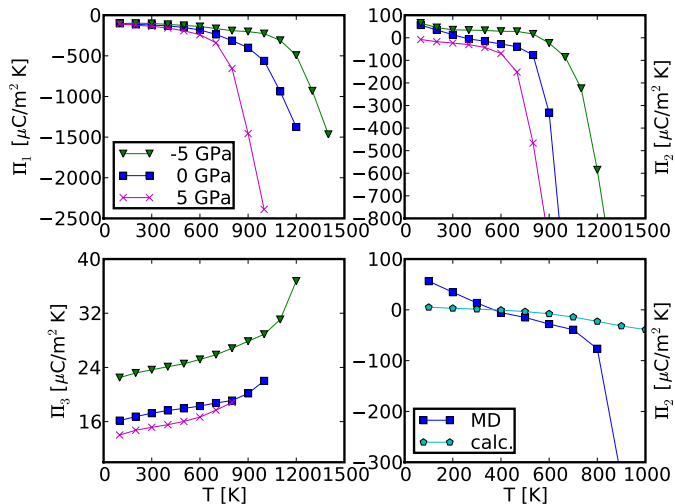


FIG. 2. Pyroelectric coefficients. Π_1 (top-left), Π_2 (top-right), Π_3 (bottom-left) for $P = -5, 0, 5$ GPa, represented by triangle, square, cross line respectively. Bottom-right panel shows Π_2 directly calculated from the MD (square line) simulations and computed with formula (pentagon line).

pute dP_s/dT , the total pyroelectric coefficient Π in Eq. 1. We also performed MD simulations in the $N\epsilon T$ ensemble (constant strain) and obtained Π_1 , and the difference gives Π_2 . We computed Π_3 from MD $N\sigma T$ simulations.

The MD simulations were carried out in a super cell with $8 \times 8 \times 8$ primitive unit cells, which is 5120 atoms (5120 cores and 5120 shells). The $N\sigma T$ ensemble allows the shape and volume to change at constant stress, by which Π and Π' can be obtained. P_s decreases with temperature and drops to zero at the phase transition to the paraelectric phase at 1200 K (Fig. 1), which agrees well with the experimental value of 1430K [22] and 1480K [1].

In order to understand the effects of volume error and the effects of pressure, we repeated the MD simulations and analysis at ± 5 GPa. We found that $P = 5$ GPa reduces the volume about 3.6%, and $P = -5$ GPa increases the volume by 4.0%. T_c is 1400 K and 1000 K for $P = -5$ and 5 GPa respectively.

We separately computed Π_1 from MD simulations in the NVT ensemble. The volume of the target temperature T_v was taken from the previous $N\sigma T$ simulations. MD simulations at $T = T_v, T_v \pm 10, T_v \pm 20$ K were carried out to calculate Π_1 at T_v in Fig. 2 and Table III. Π_1 decreases with temperature and pressures, as does Π_2 , calculated by $\Pi - \Pi_1$. We found $\Pi_2 = 13.5 \mu\text{C}/\text{m}^2\text{K}$ and $\Pi_3 = 17.6 \mu\text{C}/\text{m}^2\text{K}$ at 300 K. While lacking the direct and complete experimental data of all the coefficients of pyroelectricity, we estimate them as listed in in Table III by combining the reported data of ref.[26, 27] and [2]. There is good agreement between the experiment and present calculations.

As a check, we calculated Π_2 in an alternative way

TABLE III. comparison of pyroelectric coefficient of LiNbO_3 .

	Π'	Π	Π_1	Π_2	Π_3
Present	-90.2	-107.7	-121.3	13.5	17.6
Calc. from Exp[2, 27]	-133.0	-154.9	-171.9	17.0	21.9
Exp [32]		-83	-95.8	12.8	

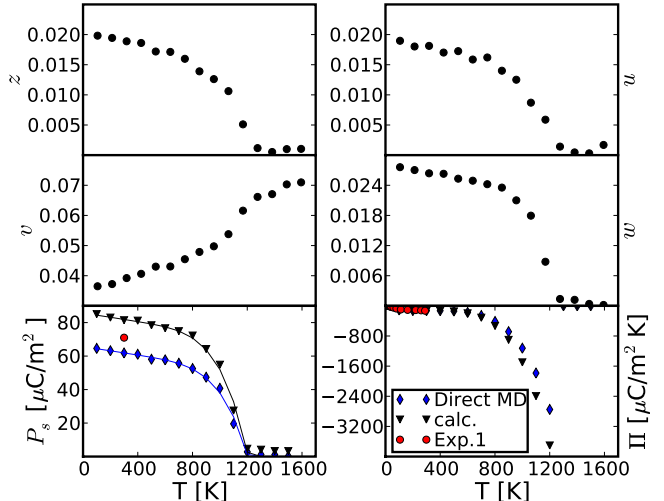


FIG. 3. The average value of z , u , v and w in MD. The P_s and Π can be calculated using z , u , v , w and Born effective charge Z^* (triangle line), compared with experiment (circle line) [2] and direct MD results (diamond line).

as $\Pi_2 = \alpha_{jk} c_{jklm} d_{3lm} = 2e_{31}\alpha_1 + e_{33}\alpha_3$ for LiNbO_3 , where e_{31}, e_{33} are piezoelectric stress constants (Voigt notation), which are obtained by the first principles calculation at zero pressure and zero temperature as listed in Table II. Using α_j obtained from $N\sigma T$ simulations, we computed Π_2 (Fig. 2), which agrees with direct MD results at low temperatures up to 700K.

We found that Π_1 is dominant and Π_3 is small. The absolute value of both Π_1 and Π_2 increase rapidly with temperature as T_c is approached.

Up until now there has not been a clear exposition of the origin of pyroelectricity and the electrocaloric effect, but they are often considered as resulting from increasing polarization disorder with temperature. We find that the effects can be understood from the changes in crystal structure with temperature, as a simple anharmonic effect. We determined the average structural parameters z , u , v and w [12] from the average atomic positions in the MD simulations (Fig. 3). We computed the P_s versus temperature using these average positions with the Born effective charges Z^* obtained from the DFPT computations, and $P_s = \frac{e}{\Omega} \sum_i Z_i^* r_i$ where r_i is the i th ionic displacement along the polar axis from the centrosymmetric to polar structures, e the elementary charge and Ω the unit cell volume (Fig. 3). The results show that the pyroelectric effect can be entirely understood in the clas-

sical regime above room temperature from the change in average structure with temperature, peaking at T_c . Thus the anharmonic internal atomic rearrangement with respect to the temperature contribute the dominant part of the pyroelectricity. We find that pyroelectric coefficients could easily be obtained experimentally without electrical measurements, simply by studying changes in crystal structure with temperature, along with first-principles theoretical effective charges Z^* . Good pyroelectrics and electrocaloric materials should have T_c slightly higher than the operating temperatures.

This work was partly supported by the EFree, an Energy Frontier Research Center funded by the U.S. Department of Energy, Office of Science, Office of Basic Energy Sciences under Award Number de-sc0001057 and partly by the Office of Naval Research No. N00014-07-1-0451.

-
- [1] M. Lines and A. Glass, *Principles and Applications of Ferroelectrics and Related Materials* (Clarendon Press, Oxford, 1977).
- [2] A. M. Glass and M. E. Lines, Phys. Rev. B **13**, 180 (1976).
- [3] M. E. Lines and A. M. Glass, Phys. Rev. Lett. **39**, 1362 (1977).
- [4] R. E. Cohen and H. Krakauer, Phys. Rev. B **42**, 6416 (1990).
- [5] R. Cohen, Nature **358**, 136 (1992).
- [6] J. D. Brownridge and S. Raboy, Journal of Applied Physics **86**, 640 (1999).
- [7] H. Ida and J. Kawai, X-Ray Spectrometry **34**, 225 (2005).
- [8] <http://www.amptek.com/coolx.html>.
- [9] B. Naranjo, J. Gimzewski, and S. Putterman, Nature **434**, 1115 (2005).
- [10] I. Inbar and R. E. Cohen, Phys. Rev. B **53**, 1193 (1996).
- [11] K. Parlinski, Z. Q. Li, and Y. Kawazoe, Phys. Rev. B **61**, 272 (2000).
- [12] M. Veithen and P. Ghosez, Phys. Rev. B **65**, 214302 (2002).
- [13] A. Rauber, "Current topics in materials science," (North-Holland, Amsterdam, 1978) p. 481.
- [14] J. F. Scott, Science **315**, 954 (2007).
- [15] G. Akcay, S. P. Alpay, J. V. Mantese, and G. A. Rossetti, Jr., Applied Physics Letters **90**, 252909 (2007).
- [16] S. Prosandeev, I. Ponomareva, and L. Bellaiche, Physical Review B **78**, 052103 (2008).
- [17] R. E. Newnham, *Properties of Materials: Anisotropy, Symmetry, Structure* (Oxford University Press, Oxford, 2005).
- [18] P. Giannozzi, S. de Gironcoli, P. Pavone, and S. Baroni, Phys. Rev. B **43**, 7231 (1991).
- [19] X. Gonze, J. M. Beuken, R. Caracas, F. Detraux, M. Fuchs, G. M. Rignanese, L. Sindic, M. Verstraete, G. Zerah, F. Jollet, M. Torrentb, A. Royb, M. Mikamic, P. Ghosezd, J. Y. Ratyd, and D. C. Allane, Computational Materials Science **25**, 478 (2002).
- [20] J. P. Perdew and Y. Wang, Phys. Rev. B **45**, 13244 (1992).
- [21] <http://opium.sourceforge.net>.
- [22] H. Boysen and F. Altorfer, Acta Crystallographica Section B: Structural Science **50**, 405 (1994).
- [23] S. H. Wemple, J. M. DiDomenico, and I. Camlibel, Applied Physics Letters **12**, 209 (1968).
- [24] V. V. Zhdanova, V. P. Klyuev, V. V. Lemanov, I. A. Smirnov, and V. V. Tikhonov, Sov. Phys.-Solid State (USA) **10**, 1360 (1968).
- [25] *Properties of Lithium Niobate*, edited by K. K. Wong (INSPEC, 2002).
- [26] Y. S. Kim and R. T. Smith, Journal of Applied Physics **40**, 4637 (1969).
- [27] R. T. Smith and F. S. Welsh, Journal of Applied Physics **42**, 2219 (1971).
- [28] H. Kaplan, Phys. Rev. **125**, 1905 (1962).
- [29] X. Sha and R. E. Cohen, Phys. Rev. B **73**, 104303 (2006).
- [30] R. Resta and D. Vanderbilt, in *Physics of Ferroelectrics: a Modern Perspective*, edited by C. Ahn, K. Rabe, and J. Triscone (Springer-Verlag, New York, 2007) pp. 31–68.
- [31] T. Yamada, N. Niizeki, and H. Toyoda, Jpn. J. Appl. Phys. **6**, 2219 (1967).
- [32] S. B. Lang, Physics today **58**, 31 (2005).
- [33] M. Sepiarsky, Z. Wu, A. Asthagiri, and R. E. Cohen, Ferroelectrics **301**, 55 (2004).
- [34] W. Smith, C. W. Yong, and P. M. Rodger, Molecular Simulation **28**, 385 (2002).